


Article

Accurate Identification for CW Direct Signal in Underwater Acoustic Ranging

Jing Li ^{1,2,3} , Jin Fu ^{1,2,3,*} and Nan Zou ^{1,2,3}

¹ National Key Laboratory of Underwater Acoustic Technology, Harbin Engineering University, Harbin 150001, China; xty2587@hrbeu.edu.cn (J.L.); zounan@hrbeu.edu.cn (N.Z.)

² Key Laboratory of Marine Information Acquisition and Security (Harbin Engineering University), Ministry of Industry and Information Technology, Harbin 150001, China

³ College of Underwater Acoustic Engineering, Harbin Engineering University, Harbin 150001, China

* Correspondence: fujin@hrbeu.edu.cn

Abstract: The underwater channel is bilateral, heterogeneous, uncertain, and exhibits multipath transmission, sound line curvature, etc. These properties complicate the structure of the received pulse, causing great challenges in direct signal identification for ranging purposes and impacts on back-end data processing, even accurate acoustic positioning. Machine learning (ML) combined with underwater acoustics has emerged as a prominent area of research in recent years. From a statistical perspective, ML can be viewed as an optimization strategy. Nevertheless, the existing ML-based direct-signal discrimination approaches rely on independent assessment, utilizing a single sensor (beacon or buoy), which is still insufficient for adapting to the complex underwater environment. Thus, discrimination accuracy decreases. To address the above issues, an accurate CW direct signal detection approach is performed using the decision tree algorithm, which belongs to ML. Initially, the pulse parameter characteristics in the underwater multipath channel are investigated and the parameter models are built. Then, based on multi-sensor localization performance feedback, fusion characteristics for diverse pulse are created. Next, the pulse parameter characteristics are preprocessed to mitigate the impact of varying magnitudes and units of magnitude on data processing. Then, the decision tree is built to obtain the desired output results and realize accurate recognition of the ranging direct signals. Finally, the feasibility and reliability of this paper's method are verified by computer simulation and field testing.

Keywords: machine learning; direct signal identification; information fusion; performance feedback



Citation: Li, J.; Fu, J.; Zou, N. Accurate Identification for CW Direct Signal in Underwater Acoustic Ranging. *J. Mar. Sci. Eng.* **2024**, *12*, 454. <https://doi.org/10.3390/jmse12030454>

Academic Editor: Sergei Chernyi

Received: 12 February 2024

Revised: 25 February 2024

Accepted: 3 March 2024

Published: 5 March 2024



Copyright: © 2024 by the authors. Licensee MDPI, Basel, Switzerland. This article is an open access article distributed under the terms and conditions of the Creative Commons Attribution (CC BY) license (<https://creativecommons.org/licenses/by/4.0/>).

1. Introduction

As ocean exploration deepens, acoustic localization is used in an increasing number of domains underwater [1–3]. Typically, underwater acoustic localization systems comprise a platform and several sensors. Sensors are organized into a sensor network based on a certain geometric configuration, and communicate with the platform through acoustic signals. Precise determination of the platform location can be achieved by measuring the parameters of the direct sound signals.

However, underwater acoustic fields are complicated and multi-path effects are severe [4–6], which leads to the fact that the received signal is the superposition of a series of pulses. The issue of effectively distinguishing the direct acoustic signal from complicated overlaid pulses is crucial for underwater acoustic localization, as well as for back-end data processing. Many related studies have been conducted to address the above issue with identification and may be broadly categorized as follows, based on the various approaches and techniques employed.

In the first category, the primary purpose is to use the correlation between received pulses to realize the identification of a direct pulse. Literature [7–9] constructed the orthogonal correlation function between the received signals and the source signals, and identified

the correlation peaks to accurately estimate the direct pulse and parameters. Xia et al. [10] constructed a spatial spectral function using the MUSIC algorithm by exploiting the orthogonality of the noise and signal subspaces to select direct signals. Nevertheless, this approach typically necessitates the centralized processing of unprocessed data via underwater acoustic communications, which is not conducive to instantaneous data processing.

In the second category, the primary technique is to separate the direct signal inside the overlaid multipath signals. Literature [11–15] used different methods to suppress the effect of the multipath and obtain the direct signal, such as multi-dimensional matching filters, the orthogonal correlation, and the energy peak searching and so on. Additionally, methods such as channel equalization, time-reversal mirrors, and homomorphic filtering can be employed to effectively suppress multipath signals within the overlapped pulses, hence facilitating the identification of the direct pulse.

The third type of method depends on the parametric characteristics. The primary method utilized in engineering applications is the artificial expert system, which establishes predetermined criteria based on various project requirements and conditions, as introduced in literature [16,17]. Nevertheless, the weighting values of manually assigned criteria lack precision, and are unsuitable for the complicated and dynamic underwater environment.

Recently, ML integrated with underwater acoustics has gained significant attention, which is a type of optimization method from the statistical perspective [18–21]. The decision tree (DT) technique is commonly used and efficient for classification in ML, depending on feature characteristics for tree construction [22–24]. Literature [25] investigated the identification method using the DT technique, depending on the independent judgment of the direct signal, abbreviated to S-DT. However, in S-DT methods, independent judgments restrict the utilization of effective information and lead to poor adaptability to complex underwater environments, especially when sharp interference or false alarm pulses exist. Hence, using features from multi-sensors may be a vital aid to enhancing the performance. Nevertheless, the process of signal detection and the estimation of various sensors are independent of each other, and the parameters cannot be directly employed for constructing decision trees.

To address the issue above, this work explores a precise identification method using DT, by integrating the fusion information from multi-sensors. Firstly, the characteristics of pulse parameters in ideal underwater acoustic multipath channels are investigated and their models are established. Secondly, the construction of fusion features is studied. The pulse parameters of different sensors cannot be directly used due to the independent detection. Hence, by exploring the correlation between the direct signals and positioning performance, a cost function is constructed using the geometric intersection principle. The fusion features of different pulses can be calculated through positioning performance feedback. Subsequently, the pulse parameter features are preprocessed to mitigate the impact of varying magnitudes and magnitude units on data processing. Then, the decision tree is constructed using the features to obtain the outputs and achieve the precise and efficient identification of direct signals. Ultimately, the efficacy and robustness of the suggested approach are confirmed by simulation and actual experimental data processing. We abbreviate the proposed method, which depends on multiple feature fusion based on localization feedback, as MFF-LF.

The structure of the paper is as follows: Section 2 examines the pulse characteristics in the underwater environment; Section 3 introduces the DT algorithm; Section 4 investigates the MFF-LF method; the simulation analysis is presented in Section 5; Section 6 presents the field test data processing; Section 7 discusses the limitation of MFF-LF; Section 8 provides the conclusion.

2. Pulse Characteristics in Underwater Environment

The underwater acoustic channel can be conceptualized as a slow time-varying coherent multi-path channel. In an ideal channel, the sound field has an equal velocity distribution, and all reflections are approximately mirror reflections. Aside from the direct

signal, there are also surface reflections, seabed reflections, and secondary reflections between the surface and seafloor in the received signals. Based on the ray acoustics [26], all reflections are assumed to be specular reflections, disregarding the impact of sound line bending. Then, the ideal multipath channel model is depicted in Figure 1.

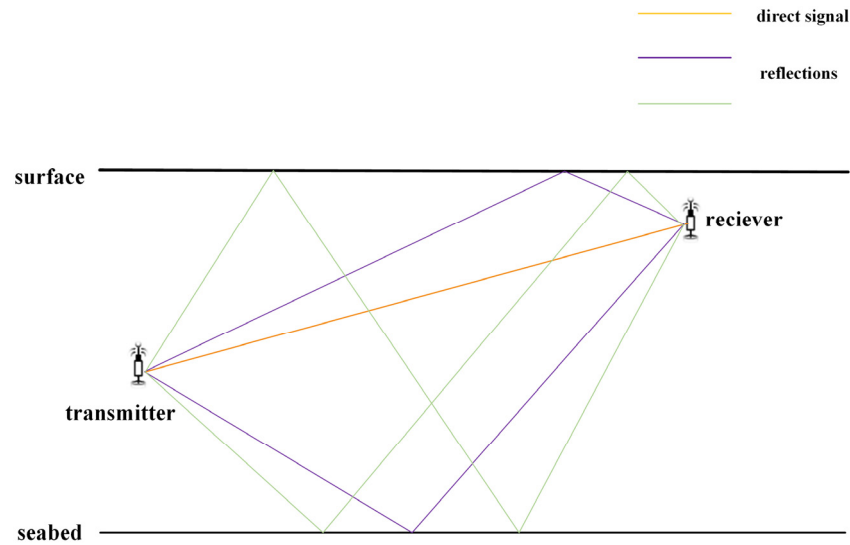


Figure 1. Ideal multipath acoustic channel model.

The source signal $s(t)$ is sent from the transmitter and travels via several paths to reach the receiver. The signal received can be mathematically represented as:

$$y(t) = \int h(\tau, t) s(t - \tau) d\tau + e(t). \tag{1}$$

In Equation (1), $e(t)$ represents the ambient noise and $h(\tau, t)$ denotes the channel impulse response function. Under ideal channel conditions, $h(\tau, t)$ can be expressed as follows [25]:

$$h(\tau, t) = \sum_{i=1}^N a_i(t) \delta(t - \tau - \rho_i \cdot (t - \tau_i)). \tag{2}$$

In Equation (2), N represents the total number of transmission paths. $a_i(t)$ and τ_i denote the amplitude and delay, respectively. ρ_i denotes the Doppler coefficient of the signal. Let the sound speed underwater be denoted by c and let v_i denote the radial velocity between the transmitter and receiver. Then, we have:

$$\rho_i = \frac{c}{c - v_i}. \tag{3}$$

By substituting Equation (2) and Equation (3) into Equation (1) and subsequently arranging the terms, we may derive the formula for the received signal.

$$y(t) = \sum_{i=1}^N a_i(t) s(\rho_i \cdot (t - \tau_i)) + e(t). \tag{4}$$

Under a multipath channel, the signal received within the signal cycle is a superposition of direct and reflected signals, as shown in Equation (4). The parameters vary, including amplitude, delay, Doppler shift, pulse width, and so on.

Subsequently, a study will be undertaken on the distinct parameter features of ranging CW pulses, building upon the background of underwater acoustic positioning, which will serve as a basis for the later development of MFF-LF algorithms.

- Delay

The delay is calculated by the ratio of signal propagation range to the sound speed. Taking one-time reflection as an example, the sound propagation paths are shown in Figure 2. In the figure, D and d_0 refer to the horizontal and the linear distance between the transmitter and receiver, respectively. H represents the depth of the water. H_{1u} and H_{2u} , respectively, represent the vertical depth from the water surface to the transmitter and receiver. H_{1b} and H_{2b} denote the vertical depth of the transmitter and receiver to the bottom of the water, separately.

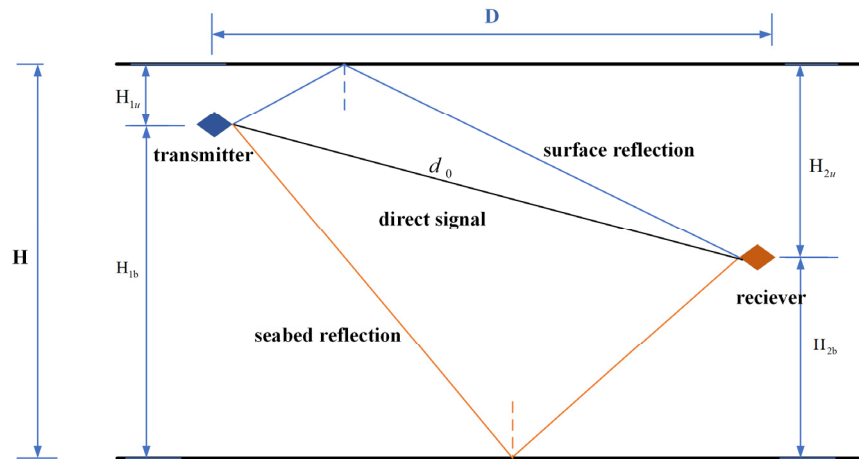


Figure 2. Diagram of propagation paths (one-time reflection).

The calculation of the time delay is given by Equation (5) to Equation (7). For direct signals, there is:

$$t_d = \frac{d_0}{c}. \tag{5}$$

The phenomenon of reflection is examined in two scenarios. If the number of reflection times is odd, the delay will be computed by the following equation:

$$t_{ru} = \frac{\left(1 + \left(\frac{D}{(i-1) \cdot H + H_1 + H_2}\right)^2\right)^{\frac{1}{2}} \cdot (H_1 + (i-1) \cdot H + H_2)}{c},$$

$$t_{rb} = \frac{\left(1 + \left(\frac{D}{(i-1) \cdot H + H_{1b} + H_{2b}}\right)^2\right)^{\frac{1}{2}} \cdot (H_{1b} + (i-1) \cdot H + H_{2b})}{c}, \tag{6}$$

where t_{ru} and t_{rb} denote the time delay for surface reflection and seabed reflection, separately. i denotes the number of reflection times.

If reflection times are even, then

$$t_{ru} = \frac{\left(1 + \left(\frac{D}{i \cdot H + H_1 - H_2}\right)^2\right)^{\frac{1}{2}} \cdot (H_1 + i \cdot H - H_2)}{c},$$

$$t_{rb} = \frac{\left(1 + \left(\frac{D}{i \cdot H + H_{1b} - H_{2b}}\right)^2\right)^{\frac{1}{2}} \cdot (H_{1b} + i \cdot H - H_{2b})}{c}. \tag{7}$$

- Amplitude

Using the ray acoustics for the analysis, the pulse amplitude can be obtained by the following equation for the direct signal:

$$A_d = \frac{1}{d_0}. \tag{8}$$

Similar to the process of analyzing the time delay, the pulse amplitude of the reflected sound is discussed in different cases. For an odd number of reflection times,

$$\begin{aligned} A_{ru} &= (ct_{ru})^{-1} \cdot \alpha_u^{\frac{i+1}{2}} \cdot \alpha_b^{\frac{i-1}{2}} \\ A_{rb} &= (ct_{rb})^{-1} \cdot \alpha_u^{\frac{i-1}{2}} \cdot \alpha_b^{\frac{i+1}{2}} \end{aligned} \quad (9)$$

where α_u and α_b denote the reflection coefficients and i denotes the number of reflection times. If reflection times are even, then

$$\begin{aligned} A_{ru} &= (ct_{ru})^{-1} \cdot (\alpha_u \cdot \alpha_b)^{\frac{i}{2}} \\ A_{rb} &= (ct_{rb})^{-1} \cdot (\alpha_u \cdot \alpha_b)^{\frac{i}{2}} \end{aligned} \quad (10)$$

• Width of pulse

If the relative motion exists between the transmitter and receiver, the received signal will exhibit a linear compression (or stretching) on the time scale. Figure 3 shows a schematic diagram of a signal received at the front and back edges in the presence of relative motion. Here, t_1 indicates the arrival time of the pulse front and t_2 indicates the arrival time of the pulse back edge. v indicates the velocity of the platform (receiver). The width of the emitted pulse is T . The width of the received pulse is τ .

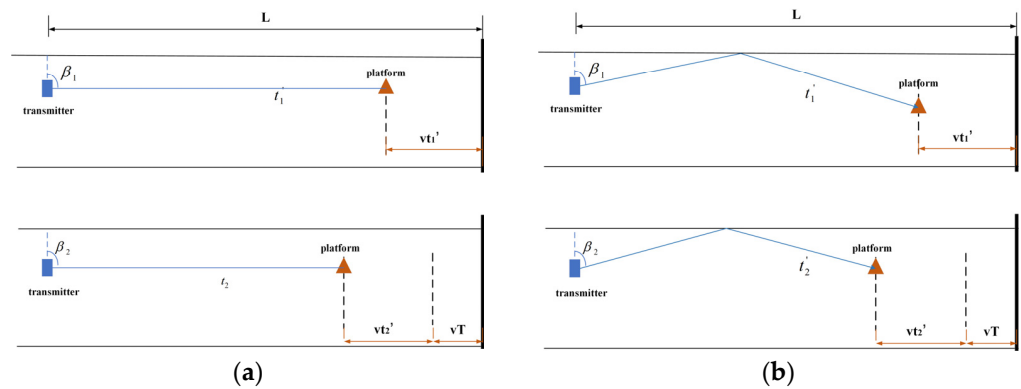


Figure 3. Diagram of received signals considering relative motion (a) direct signal; (b) reflected signal.

For a direct signal,

$$\begin{aligned} t_1 &= \frac{L}{v+c} \\ t_2 &= \frac{L-vT}{v+c} \end{aligned} \quad (11)$$

$$\tau = T - (t_1 - t_2) = \left(1 - \frac{v}{v+c}\right)T. \quad (12)$$

Due to the fact that $v \ll c$, the width τ can be calculated as

$$\tau \approx \left(1 - \frac{v}{c}\right)T. \quad (13)$$

For the reflected, taking the surface reflection as an example,

$$\begin{aligned} t'_1 &= \frac{L}{v+c \sin \beta_1} \\ t'_2 &= \frac{L-vT}{v+c \sin \beta_2} \end{aligned} \quad (14)$$

Since $\beta_1 \approx \beta_2$, then the width of the reflected pulse can be written as

$$\tau' = T - (t'_1 - t'_2) = \left(1 - \frac{v}{c \sin \beta_1}\right)T. \quad (15)$$

- Doppler shift

The Doppler shift occurs when there is a relative motion between the transmitter and the receiver, which causes changes in the received signals on both the time scale and in the waveform, specifically resulting in a shift in the signal's frequency.

According to the analysis of the pulse width above, the Doppler shift of direct signals and the one-time reflections can be obtained as Equations (16) and (17).

$$f_d = f_0 \frac{v}{c} \tag{16}$$

$$f'_d = f_0 \frac{v}{c \sin \beta_1}, \tag{17}$$

where f_0 denotes the frequency of the transmitted CW signal.

Overall, by studying the pulse characteristics in ideal acoustic channels, different parameter models have been constructed, which is of great significance for subsequent research on the accurate identification of ranging direct signals. This research will examine the identification approach based on DT, utilizing the pulse characteristics investigated above.

3. The DT Algorithm

This section focuses on the fundamentals of the DT algorithm. The CART decision tree [27,28] is used in this research and the Gini Index is employed to determine the classification attributes.

Let the sample set be defined as D . y denotes the number of sample classifications ($k = 1, 2, \dots, y$). p_k represents the proportion of the k -th class of samples to the sample set D . The purity of the sample set D can be measured by the value $Gini(D)$, which is expressed as follows:

$$Gini(D) = \sum_{k=1}^y \sum_{k' \neq k} p_k p_{k'} = 1 - \sum_{k=1}^y p_k^2. \tag{18}$$

Equation (18) denotes the probability that two samples randomly selected from the sample do not share the same category. The purity of D increases as $Gini(D)$ decreases.

Define the attribute set $H = \{h_1, h_2, \dots, h_M\}$. M denotes the number of characteristic attributes. Then, the Gini coefficient of attribute h can be expressed as Equation (19).

$$GI(D, h) = \sum_{m=1}^M \frac{|D^m|}{|D|} Gini(D^m). \tag{19}$$

In Equation (19), D^m denotes the set of the samples characterized by the attribute h_m . The optimal segmentation attributes h_* are determined as follows:

$$h_* = \operatorname{argmin}_{h \in H} GI(D, h). \tag{20}$$

Branches are generated for each value of h_* , and are then recursively evaluated until the last node of the decision tree is formed to finish the creation.

4. The MFF-LF Method

Learning from the previous section, the selection of feature attributes greatly impacts the performance of DT. This paper will then investigate the MFF-LF method in the following two respects. One is the method for the construction of fusion features based on localization feedback by using multi-sensor information. Another is the method for preprocessing feature parameters. The underwater localization scene is shown in the following figure.

As shown in Figure 4, within each signal transmission period, the platform emits CW pulses, and the sensors receive the signal and then complete the measurement of the pulse parameters. Let s denote the position of the sensors, x denote the target position, and c the

sound speed. Then, according to the geometric intersection localization principle, there is the following relationship:

$$\|s - x\|_2 = c \cdot t. \tag{21}$$

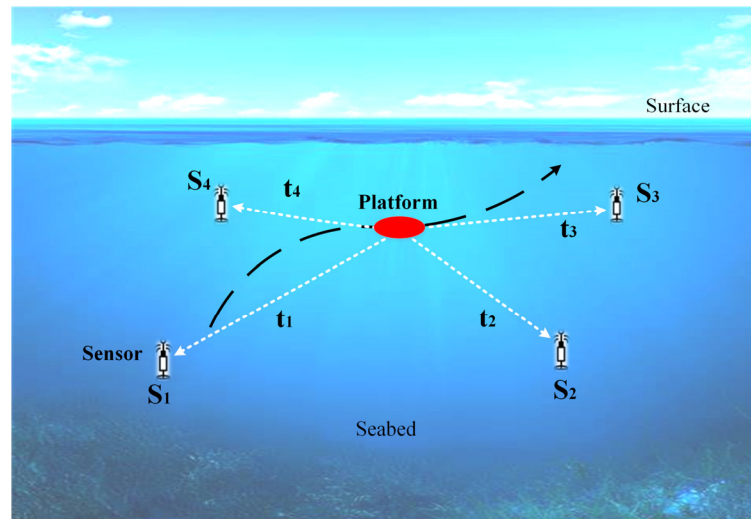


Figure 4. Scene of underwater localization.

In Equation (21), $\|\cdot\|_2$ denotes the Euclidean paradigm and the formula is in matrix form, then it is turned into another form using the coordinates, as follows:

$$(x - x_i)^2 + (y - y_i)^2 + (z - z_i)^2 = (ct_i)^2. \tag{22}$$

4.1. Construction of Fusion Feature

To solve Equation (22), the optimization algorithm, like the Differential Evolution method, the Gauss–Newton method, and so on, can be used. No matter what kind of techniques are chosen to optimize the problem, the core issue is to establish the cost function, as shown below.

$$\hat{x} = \min f_{obj}(x). \tag{23}$$

Equation (23) shows that, when the function $f_{obj}(x)$ takes the minimum value, the target position x takes the optimum value. Theoretically, if there are no measurement errors, then

$$f_{obj}(\hat{x}) = 0. \tag{24}$$

The specific formula expression in $f_{obj}(x)$ varies depending on the selected criteria. If the minimum mean square error criterion is selected, then $f_{obj}(x)$ can be expressed as follows:

$$f_{obj}(x) = \sqrt{\sum_{i=1}^4 ((x - x_i)^2 + (y - y_i)^2 + (z - z_i)^2 - (ct_i)^2)}. \tag{25}$$

In the issue of identifying direct signals, if all the correct direct pulses are successfully picked out the to participate in the subsequent solution, then the minimum value of $f_{obj}(x)$ can be achieved. Otherwise, wrong identification will increase the value of the cost function due to the geometrically infeasible intersection. Thus, in a given signal cycle, the likelihood of identifying the pulse that minimizes the cost function $f_{obj}(x)$ as the direct pulse is greater than that of other pulses.

Applying the above thought, we next investigate how to utilize the multi-sensor information to create fusion features based on location feedback, which is beneficial for improving the performance of DT.

Let the pulses of each sensor be sorted in the sequential order, separately, and the number of pulses received within the signal period by various sensors be marked as m_1, m_2, m_3, m_4 . Then, choosing one pulse from each sensor to create a group set \tilde{t} and taking four sensors ($N = 4$) as an example, if the serial numbers are marked as l, j, k, h , then \tilde{t} is as follows:

$$\tilde{t} = \{t_{1l}, t_{2j}, t_{3k}, t_{4h}\} \tag{26}$$

$$l, j, k, h \in \{Num \mid 0 < Num \leq m_i, Num \in \mathbb{N}_+\}, \tag{27}$$

where t_{1l} denotes the delay of the l -th pulse detected by sensor 1#. Let i denote the sensor number. Then, set \tilde{t} has a total of $\prod m_i$ combinations, which form the set $\tilde{T} = \{\tilde{t}_1, \tilde{t}_2, \dots, \tilde{t}_{\prod m_i}\}$, as seen in Figure 5.

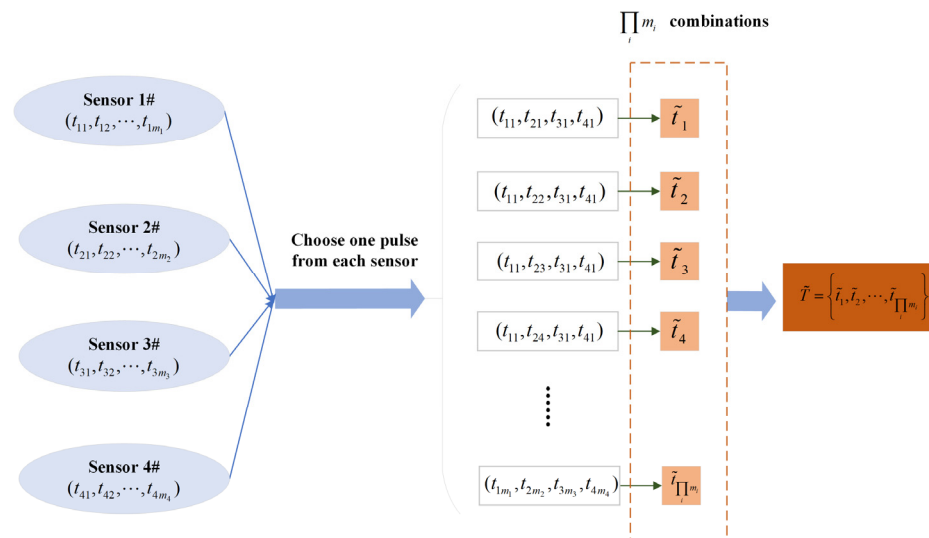


Figure 5. Combinations of signals from multi-sensors.

The cost function f_{obj} is built according to the minimum mean square error criterion.

$$f_{obj} = \min_i \sum (\|s_i - x\|_2 - c \cdot \tilde{t})^2 \quad i = 1 \cdots N. \tag{28}$$

According to Equation (28), if f_{obj} goes to the minimum value, the correct pulse set $t^* = \{t_{1c}, t_{2c}, t_{3c}, t_{4c}\}$ will be found. Among the set, t_{ic} means the correct direct signal of the sensor i #. Further processing must be performed before we obtain t^* , due to the interaction between the multi-sensors' fusion.

For each combination in \tilde{T} , Equation (28) will give the calculation of the function values. The number of values is $\prod m_i$. Different combinations correlate to varying values of f_{obj} . It is necessary to determine the role of a certain pulse, for example t_{11} . According to the combinations in Figure 5, t_{11} appears in more than one set. All combinations containing t_{11} should be extracted from \tilde{T} , and then form a new collection \tilde{T}_{11} , seen as Figure 6.

Combined with Figure 6, the formula for summarizing the aforementioned categorization procedure is as shown in Equation (29).

$$\begin{cases} \tilde{T}_{ip} \cap \tilde{T}_{iq} = \emptyset & (p \neq q \ \& \ p, q = 1, 2, \dots, m) \\ \tilde{T}_1 \cup \tilde{T}_2 \cup \dots \cup \tilde{T}_m = \tilde{T} \end{cases} \tag{29}$$

The set of pulses $\{\tilde{T}_{i1}, \dots, \tilde{T}_{ip}, \dots, \tilde{T}_{im}\}$ is complete and the elements inside are mutually exclusive to each other. \tilde{T}_{ip} denotes the complete set of combinations containing the p -th pulse detected by sensor i # within the signal period.

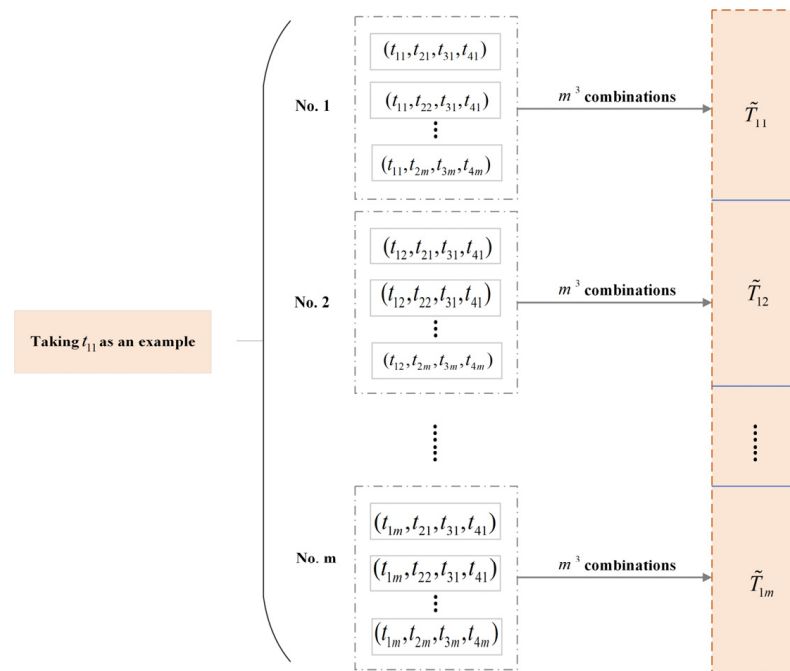


Figure 6. Recombination of signal set.

Then, the sum values of the cost function corresponding to the elements in the set \tilde{T}_{ip} are given by Equation (30), where F_{ip} is seen as the fusion feature of the pulse t_{ip} .

$$F_{ip} = \sum f_{obj}(l) \quad l \in \tilde{T}_{ip}. \tag{30}$$

From Equation (30), a new feature F_{ip} for the CW pulse is built based on the multi-sensor fusion information and the performance feedback of underwater positioning. For the pulse t_{ip} , its fusion feature F_{ip} contains the outcome of the collaborative influence of the parameter’s information from the other sensors. From the perspective of decision tree construction, the available pulse feature information dimension has increased by one dimension, from the λ dimension to the $\lambda + 1$ dimension. Overall, F_{ip} effectively links the pulse of independent sensors with each other, hence enhancing the effective information for direct pulse identification.

4.2. Preprocessing Method of Features

For the issue of identifying the direct signals, the decision tree produces a classification result, indicating whether a pulse is classified as a direct signal or not. The input of the tree is the pulses’ attributes information, with parameters that vary in amplitude and units. Data preprocessing is essential for eliminating the effect of varying magnitudes among distinct characteristics and enhancing the performance of the decision tree.

First, the processing of a continuous value is required. Since the feature attributes, such as delay, amplitude, width, and Doppler shift are continuous and non-finitely available, they cannot be directly used for node partitioning of the decision tree. Thus, this work utilizes the bisection approach to handle the continuous values of non-discrete characteristics. The processing procedure is as follows:

The values of continuous attribute φ in the sample set D are listed in decreasing order and are stored as $\{\varphi_1, \varphi_2, \dots, \varphi_n\}$. Then, the partition nodes are obtained by using the bisection technique for discrete processing.

$$\phi_\varphi = \left\{ \frac{\varphi_i + \varphi_{i+1}}{2} \mid 1 \leq i \leq n - 1 \right\}. \tag{31}$$

Using Equation (21), the Gini coefficient is calculated for each element in the set ϕ_φ and the element with the smallest Gini coefficient is used as the optimal discrete division point for the attribute φ .

Subsequently, data preprocessing of pulse parameters is needed to make the decision tree more robust and better performing. According to the pulse characteristic investigated in Section 2, the preprocessing procedure is as follows:

- Delay

In the process constructing the decision tree, the relative size connection between various pulses' delays has greater significance than their absolute values. Thus, for each sensor i , the delay information is acquired by the subsequent process of differentiation:

$$t' = \frac{|t - t_{\min}|}{T}, \tag{32}$$

where T denotes the transmit period of the signal, and t_{\min} is the minimum value of the delay within the transmit period.

- Amplitude

Since the acoustic range of direct signals varies, the energy loss is different. There is a difference in the magnitude of the pulse amplitude. Therefore, for each sensor, a normalization is conducted:

$$A' = \frac{A}{A_{\max}}, \tag{33}$$

where A_{\max} indicates the maximum amplitude within the transmit period.

- Doppler shift

The Doppler shift is normalized as follows:

$$f' = \frac{|f - f_0|}{f_0}. \tag{34}$$

In the equation, f_0 denotes the frequency of the transmitted signal and f denotes the frequency of the received pulse signal within the transmit period.

- Fusion feature in MFF-LF

The relative size of fusion features counts. Therefore, the following difference processing is taken for the fusion features Ψ :

$$\Psi' = |\Psi - \Psi_{\min}|, \tag{35}$$

where Ψ_{\min} denotes the minimum value of the pulse from the same sensor within the transmit period.

- Width

As with the time delay, the relative size connection between various pulses' width has greater significance than their absolute values. Thus, for each sensor i , the pulse width information is acquired by the subsequent process of differentiation:

$$\tau' = |\tau - \tau_{\min}|, \tag{36}$$

where τ_{\min} is the minimum value of the delay within the transmit period.

Finally, it is also necessary to determine the label of the decision tree used for indicating the direct signals. In the MFF-LF method, the label of direct sound is recorded as 1, while the non-direct sound is recorded as 0.

In summary, the schematic diagram of the MFF-LF method proposed in this paper is summarized as Figure 7.

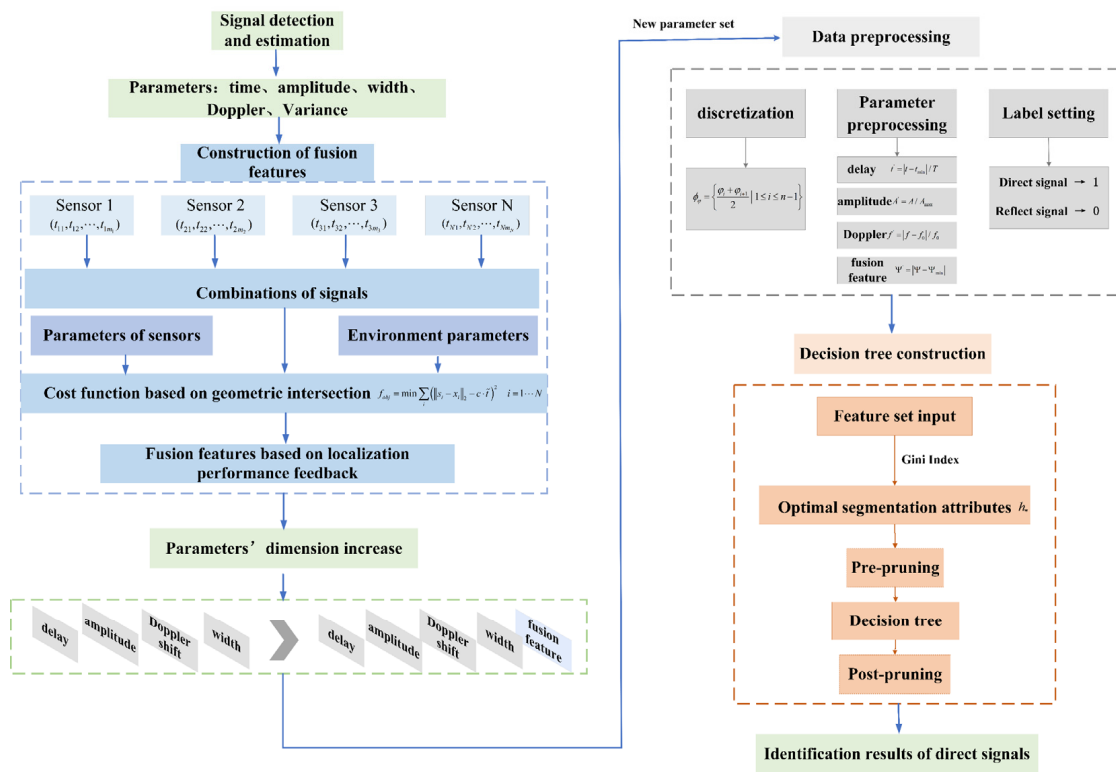


Figure 7. Schematic diagram of the MFF-LF method.

5. Simulation Analysis

In this section, computer simulation is used to simulate the received signals based on the attributes' characteristics and the acoustic propagation theory studied in Section 2 to verify the performance of the MFF-LF method under different conditions.

First, the sound field hypothesis is as follows: assuming that the acoustic field conforms to the ray acoustic theory, with only specular reflections from the water surface and the bottom taken into account. There is no absorption attenuation in the channel, only spherical wave extension attenuation. The sound velocity is uniformly distributed throughout the channel, and the background noise is Gaussian white noise.

Next, the simulation procedure for the pulse parameters is given as follows: the width of the CW signals is 10 ms; the frequency f_0 is taken as 10 kHz; the sound speed c is 1500 m/s; the depth of water, the transmitter, and the receiver are 200 m, 10 m, and 120 m, respectively; the reflection coefficient of the water surface is taken as -1 and that of the water bottom is 0.2; and the maximum number of reflections is set as 2. Coordinates of the sensors are set as shown in Table 1.

Table 1. Coordinates of sensors.

Sensor	Coordinates (m)
S1	(0, 0)
S2	(1000, 0)
S3	(1000, 1000)
S4	(0, 1000)

Assuming that the platform moves along the direction of a heading angle of 30° from the initial position (250, 250) m with a constant speed of 2 m/s, the platform's maneuvering situation is shown in Figure 8.

Under the conditions of the above simulation parameter settings, the values of delay, amplitude, width, and Doppler shift of the 500-frame received pulse are shown in Figure 9.

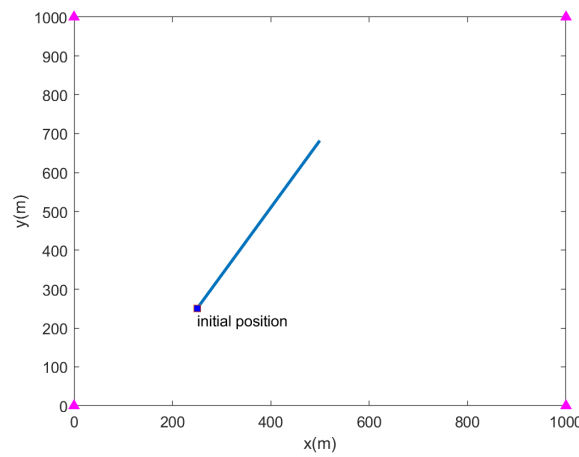


Figure 8. Situation of moving platform.

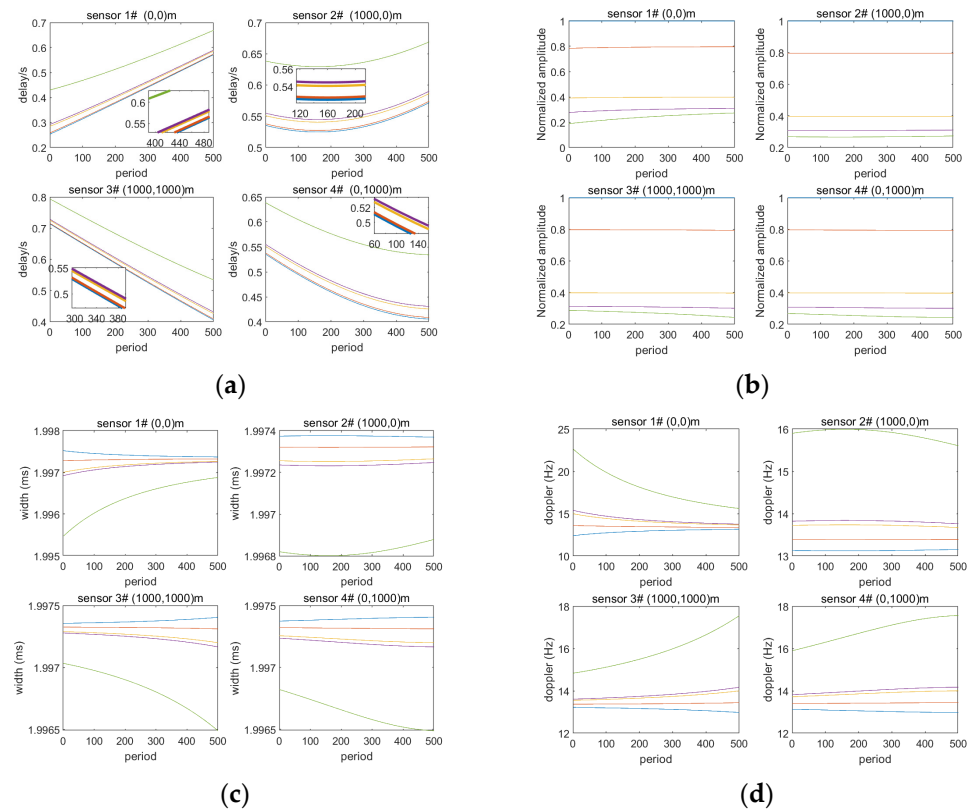


Figure 9. Parameters of received pulse (a) delay; (b) normalization amplitude; (c) width; (d) Doppler shift.

Let N_D represent the total number of received signals. m_{direct} and $m_{reflect}$ denote the number of correct identifications for direct signals and reflect signals, separately. Then, the performance evaluation metric accuracy rate is as follows:

$$\text{accuracy rate} = \frac{m_{direct} + m_{reflect}}{N_D}. \tag{37}$$

Then, the performance of the MFF-LF method will be investigated, comparing with the S-DT method. In the simulation, the delay t , amplitude A , width τ , Doppler shift f_d , and the fusion feature ψ of the pulses are selected as the parameter set of the decision tree.

According to Equation (28), the construction of the fusion feature of the MFF-LF method is based on localization performance feedback, and is therefore affected by measure-

ment errors of delay, sound velocity c , and sensor position errors x . The error parameters are set as shown in Table 2. The other parameters are set as above.

Table 2. Parameters of error sources.

δ_t	δ_A	δ_τ	δ_{f_d}	δ_c	δ_x
1 ms	2 dB	0.1 ms	1 Hz	0.5 m/s	1 m

In the total of 500 frames of data, the first 200 frames will be used as training data for the DT method and the last 300 frames are used as test data. Then, the results of different sensors are given as shown in Table 3.

Table 3. Accuracy rate of the two methods.

	S1	S2	S3	S4
MFF-LF	99.38%	100.00%	99.69%	100.00%
S-DT	97.84%	96.91%	98.92%	98.00%

Upon examining Table 3, it can be seen that, overall, the MFF-LF algorithm, as suggested in this research, successfully achieves accurate identification of direct signals, and its performance is improved compared to S-DT. Given the specified simulation settings above, for the MFF-LF method, S2 and S4 exhibit perfect accuracy in distinguishing between direct and reflected sounds, but S1 and S3 have four and two incorrect pulse data judgments, respectively. In contrast, there are 14, 22, 7, and 13 incorrect frames, respectively, which the direct signal could not correctly pick for the S-DT method. Upon reviewing the results, both algorithms experience the issue of incorrectly distinguishing the reflected sound nearest to the direct sound pulse in specific frames, which will result in an increase of errors in the subsequent data processing.

Next, we will further analyze the effect of measurement error variation on the performance of the MFF-LF method. It is assumed that σ_t , σ_c , and σ_x vary from 0 to 2 ms, 0 to 5 m/s, and 0 to 4 m, respectively. Figure 10 presents the trend of the variation.

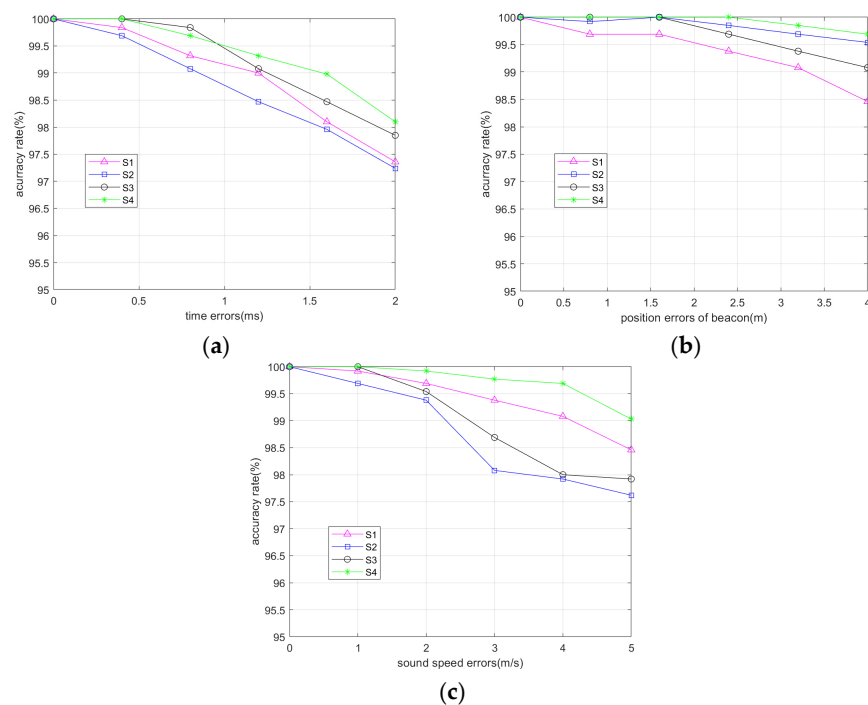


Figure 10. Changes of accuracy rate under the influence of different errors (a) σ_t ; (b) σ_x ; (c) σ_c .

Analyzing Figure 10, it can be seen that the MFF-LF algorithm exhibits the highest level of sensitivity to variations in σ_t compared to other measurement errors, as indicated by the three graphs. With the gradual increase of σ_t , the accuracy rate of various sensors decreases to varying extents. Taking S1 as an example, if there is no σ_t , the algorithm can correctly distinguish between direct sound and reflected sound with 100% precision. However, when σ_t is 2 ms, the accuracy decreases to 95.27%. Then, upon studying Figure 10b,c, it can be seen that the MFF-LF algorithm is less affected by σ_c and σ_x . The algorithm can maintain an accuracy of 98.46% even when they reach 5 m/s and 4 m, respectively.

To summarize, the simulation in this section applies the simulation data that adhere to the theoretical law to validate the feasibility of the proposed MFF-LF algorithm. Furthermore, it demonstrates that the identification accuracy of MFF-LF is enhanced in comparison to the S-DT method.

6. Field Test Data Processing

To further verify the performance of the MFF-LF algorithm, the measured data from the field test are used to verify the robustness compared with the S-DT method.

The data in this section are derived from the cooperative high-frame-rate positioning system for underwater targets. The test was conducted on 24 October 2015 at Songhua Lake, Jilin Province. The water depth was 60 m and the average sound velocity was 1460 m/s according to the hydrological conditions measured on that day. The system consists of four buoys and cooperative targets, as is shown in Figure 11. GPS antennas are mounted on the top of buoys and targets, which can be used to determine their positions in real time. Clock synchronization is maintained between the target and each buoy. The signal transmission period was 0.1 s. In each period, the target transmitted a CW pulse with a width of 10 ms. Buoys detected the signal and measured the corresponding parameters.

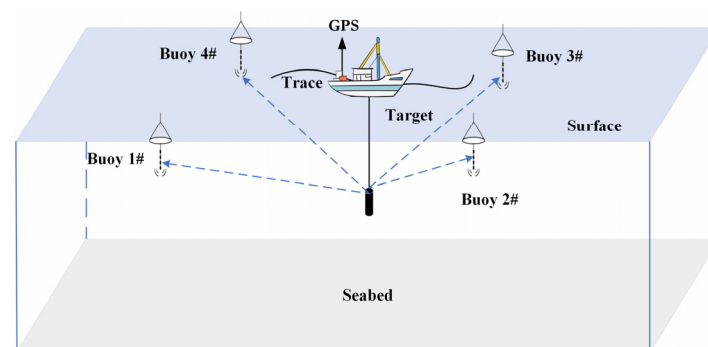


Figure 11. Situation of the field test.

Four buoys were placed in a rectangular distribution to form a measurement area with coordinates 1# (756, -41) m, 2# (-182, -11) m, 3# (-176, -1014) m, and 4# (741, -1030) m. The depth of the transmitter on the target was 3 m. The trajectory of target is shown in Figure 12.

In the total 400 frames of data, the first 150 frames will be used as training data for the DT method and the last 250 frames are used as test data. The measured delays of various buoys are shown in Figure 13.

Analyzing Figure 13, it can be seen that, due to the effect of the multipath channel, each buoy will receive several pulses within the period, including direct sound and reflected sound. Then, we will analyze the performance of the MFF-LF method, and compare it with the S-DT method. Table 4 shows the accuracy rate of the two methods and the root mean square error (RMSE) of localization. Figure 14 shows the calculation results of the target trajectory.

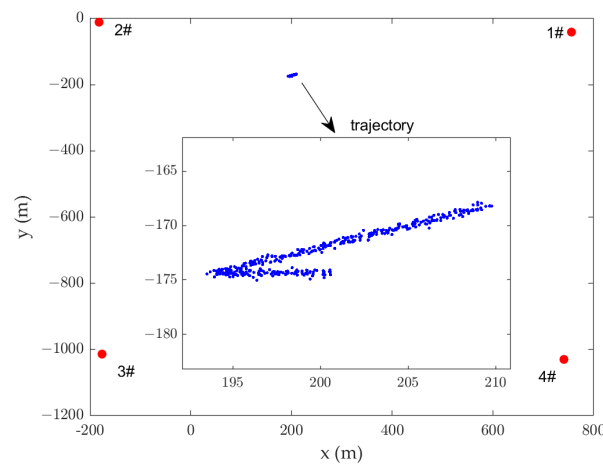


Figure 12. Trajectory of target.

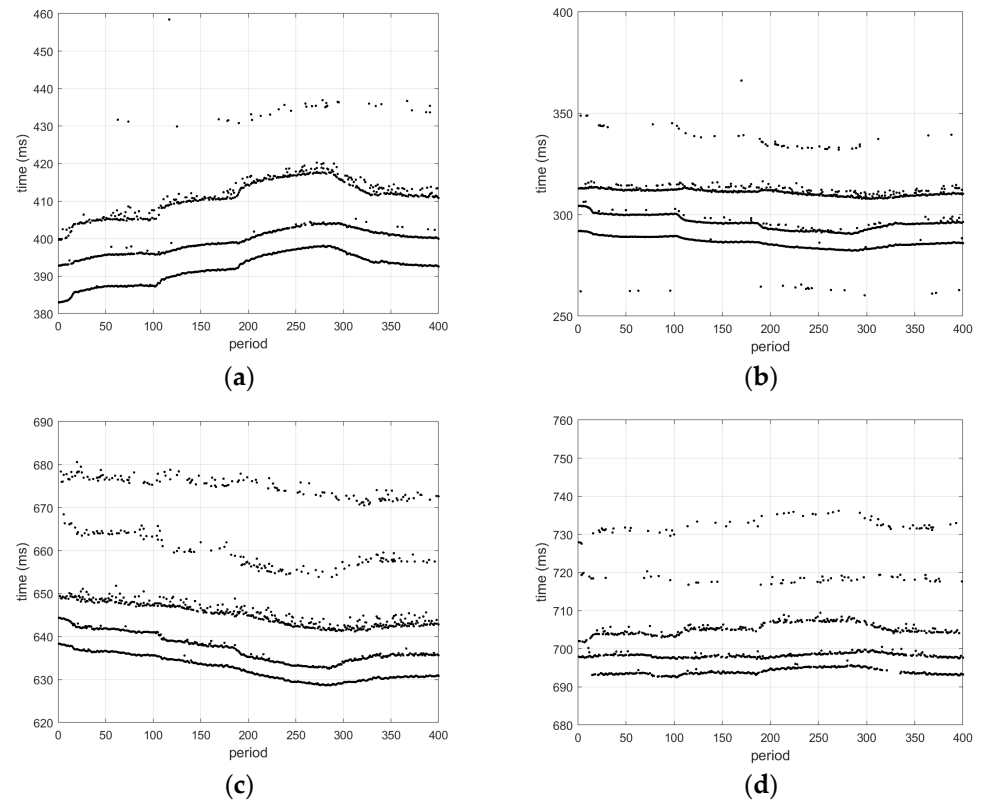


Figure 13. Measured delays of various buoys (a) sensor 1; (b) sensor 2; (c) sensor 3; (d) sensor 4.

Table 4. Accuracy rate.

	S1	S2	S3	S4	Process Time	RMSE
MFF-LF	100.00%	99.20%	98.45%	99.14%	7.23 s	2.7009 m
S-DT	97.00%	96.84%	95.10%	97.53%	2.01 s	4.8734 m

Analyzing Table 4, it is evident that the MFF-LF algorithm has demonstrated an enhanced performance compared to the S-DT algorithm in terms of identification accuracy rate. For each buoy, the accuracy rate of the MFF-LF algorithm has increased to a certain degree. By comparing the process time of the two methods, the duration of the MFF-LF method is longer than that of the S-DT method due to the fact that it takes time to handle

the fusion feature construction. The time sacrifice of the MFF-LF method can be tolerated as it brings an improvement in the performance of the direct sound recognition. Upon further examination of Figure 14, it is shown that the trajectories solved by the MFF-LF algorithm closely align with the theoretical values, with a localization RMSE of 2.7009 m, whereas the S-DT approach is 4.8734 m. Hence, the MFF-LF algorithm has performance advantages in terms of localization accuracy.

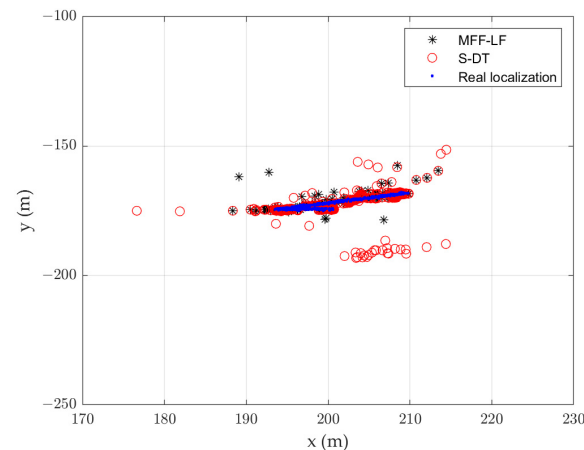


Figure 14. Solving result of the trajectory.

The field test further verifies the feasibility of the MFF-LF algorithm and its robustness in the outfield environment.

7. Discussions of the Limitation of MFF-LF

This section addresses the main limitation of the proposed method when applied to the issue of identifying the direct signals.

The key idea of the MFF-LF method is to establish the fusion feature based on the feedback of the localization performance. It is evident that the performance of MFF-LF will be affected by localization. We will analyze the limitations in terms of the following aspects.

- Limited by the measurement errors

Based on the investigation, measurement errors are one of the main factors affecting positioning accuracy, which further influence the calculation of fusion features. According to the results of the sensitivity analysis in the simulation, as measurement errors increase, the identification accuracy rate decreases to a certain extent. Hence, this algorithm has requirements for the measurement accuracy of parameters like time delay, sound speed, and sensor positions.

- Constrained by the spatial position of the platform (receiver)

In the issue of underwater acoustic localization, the localization errors vary in terms of the spatial distribution. The localization errors vary in terms of distinct spatial positions. Therefore, the performance feedback is also affected by the spatial position of the platform (receiver).

- Inferior in computational time

According to the process time of the two methods shown in Table 4 in the field test data processing, extra time is needed to handle the fusion feature construction. The time sacrifice of the MFF-LF method can be tolerated as it brings an improvement in the performance of the direct sound recognition.

8. Conclusions

Influenced by the underwater acoustic multipath channel, the signal will be distorted during transmission. The superposition of direct signals and the reflected signals results in

the intricate blending of received signals, hence complicating the identification of direct signals for acoustic ranging. In this paper, the above problems are studied, and the identification method is proposed. Then, the following conclusions are obtained:

Through analyzing the pulse parameters under the influence of multipath channels, this paper explores the correlation between parameter characteristics and positioning performance. Multi-sensor fusion features are constructed based on the principle of geometric intersection. This feature enhances the available dimensions of parameters and increases the effective information of direct sound pulses, which is beneficial for improving the performance of the decision tree.

The computer simulation calculates the features of the received pulse parameters based on the models studied in this paper. The simulation is used to verify the viability of the MFF-LF method in solving the issue of the identification of direct CW signals. The processing of field test data provides additional evidence of the feasibility of the MFF-LF method in handling complex real-world environments.

Through a comparison with the S-DT method, the proposed method can significantly boost the accuracy of direct signal identification and therefore improve the accuracy of the subsequent localization solution.

Author Contributions: Conceptualization, J.L.; Methodology, J.L. and J.F.; Software, N.Z.; Validation, J.L. and N.Z.; Formal analysis, J.F.; Writing—original draft, J.L.; Writing—review & editing, J.L., J.F. and N.Z.; Funding acquisition, J.F. All authors have read and agreed to the published version of the manuscript.

Funding: This research was funded by the Natural Science Foundation of China, grant number 62271162, and the Natural Science Foundation of China, grant number 62301182.

Data Availability Statement: The data that support the findings of this study are available from the corresponding author, [J.F.], upon reasonable request.

Conflicts of Interest: The authors declare no conflict of interest.

References

- Zhang, B.; Ji, D.; Liu, S.; Zhu, X.; Xu, W. Autonomous Underwater Vehicle navigation: A review. *Ocean. Eng.* **2023**, *273*, 113861.
- Jalal, F.; Nasir, F. Underwater navigation, localization and path planning for autonomous vehicles: A review. In Proceedings of the 18th International Bhurban Conference on Applied Sciences and Technologies, IBCAST 2021, Islamabad, Pakistan, 12–16 January 2021; pp. 817–828.
- Reggiannini, M.; Moroni, D. The use of saliency in underwater computer vision: A review. *Remote Sens.* **2021**, *13*, 26. [[CrossRef](#)]
- González-García, J.; Gómez-Espinosa, A.; Cuan-Urquizo, E.; García-Valdovinos, L.G.; Salgado-Jiménez, T.; Cabello, J.A.E. Autonomous Underwater Vehicles: Localization, Navigation, and Communication for Collaborative Missions. *Appl. Sci.* **2020**, *10*, 1256. [[CrossRef](#)]
- Li, X.P.; Wang, H.; Wang, J.; Tai, Y.; Li, C.; Yang, F. Quantitative analysis of deep-sea underwater acoustic multipath channel quality. In Proceedings of the OCEANS Hampton Roads Conference, Hampton Roads, VA, USA, 17–20 October 2022.
- Yang, T.C. Communication channels in shallow water. *J. Acoust. Soc. Am.* **2012**, *131*, 129–145. [[CrossRef](#)] [[PubMed](#)]
- Zhao, Y.; Yu, H.; Wei, G.; Ji, F.; Chen, F. Parameter estimation of wideband underwater acoustic multipath channels based on fractional Fourier transform. *IEEE Trans. Signal Process.* **2016**, *64*, 5396–5408. [[CrossRef](#)]
- Luong, N.S.; Pätzold, M. A method to estimate the path gains and propagation delays of underwater acoustic channels using the arrival phase information of the multipath components. *Int. J. Electron. Commun.* **2017**, *73*, 129–138.
- Gruden, P.; Nosal, E.M.; Oleson, E. Tracking time differences of arrivals of multiple sound sources in the presence of clutter and missed detections. *J. Acoust. Soc. Am.* **2021**, *150*, 3399–3416. [[CrossRef](#)] [[PubMed](#)]
- Xia, Z.; Li, X.; Meng, X. High resolution time-delay estimation of underwater target geometric scattering. *Appl. Acoust.* **2016**, *114*, 111–117. [[CrossRef](#)]
- Bell, B.; Ewart, T. Separating multipaths by global optimization of a multidimensional matched filter. *IEEE Trans. Acoust. Speech Signal Process.* **1986**, *34*, 1029–1037. [[CrossRef](#)]
- Anower, M.S.; Chowdhury, S.A.H.; Giti, J.E. Mitigating the effect of multipath using cross-correlation: Application to underwater network cardinality estimation. *IJSCC* **2016**, *7*, 197–220. [[CrossRef](#)]
- Liu, H.; Yang, B.; Pang, C. Multiple sound source localization based on TDOA clustering and multi-path matching pursuit. In Proceedings of the 2017 IEEE International Conference on Acoustics, Speech and Signal Processing, New Orleans, LA, USA, 5–9 March 2017; pp. 3241–3245.

14. Stoica, L.; Rabbachin, A.; Oppermann, I. A low-complexity noncoherent IR-UWB transceiver architecture with TOA estimation. *IEEE Trans. Microw. Theory Tech.* **2006**, *54*, 1637–1646. [[CrossRef](#)]
15. Guvenc, I.; Sahinoglu, Z. Threshold-based TOA estimation for impulse radio UWB systems. In Proceedings of the 2005 IEEE International Conference on Ultra-Wideband, Zurich, Switzerland, 5–8 September 2005; pp. 420–425.
16. Yu, P.; Wu, B.; Xie, S. A pulse selection method of acoustic positioning signal. *Ship Electron. Eng.* **2012**, *32*, 122–123+130.
17. Xu, Y. *Method and Software Implementation of Positioning for Buoy-Based USBL*; Harbin Engineering University: Harbin, China, 2018; pp. 31–37.
18. Zhu, X.; Dong, H.; Rossi, P.S.; Landrø, M. Feature selection based on principal component regression for underwater source localization by deep learning. *Remote Sens.* **2021**, *13*, 16. [[CrossRef](#)]
19. Zhang, W.; Wu, Y.; Lin, Y.; Ma, L.; Han, K.; Chen, Y.; Liu, C. Underwater target detection based on machine learning. In Proceedings of the 3rd IEEE International Conference on Information Communication and Signal Processing (ICICSP), Shanghai, China, 12–15 September 2020.
20. Yang, H.; Byun, S.-H.; Lee, K.; Choo, Y.; Kim, K. Underwater acoustic research trends with machine learning: Active SONAR applications. *J. Ocean. Eng. Technol.* **2020**, *34*, 277–284. [[CrossRef](#)]
21. Han, J.; Shoeiby, M.; Malthus, T.; Botha, E.; Anstee, J.; Anwar, S.; Wei, R.; Armin, M.A.; Li, H.; Petersson, L. Underwater image restoration via contrastive learning and a real-world dataset. *Remote Sens.* **2022**, *14*, 22. [[CrossRef](#)]
22. Coadou, Y. Boosted decision trees and applications. In *3rd IN2P3 School of Statistics*; E D P Sciences: Autrans, France, 2012.
23. Somvanshi, M.; Chavan, P.; Tambade, S.; Shinde, S.V. A review of machine learning techniques using decision tree and support vector machine. In Proceedings of the 2nd International Conference on Computing, Communication, Control and Automation (ICCUBEA), Pune, India, 12–13 August 2016.
24. Yang, C.; Wu, G.; Ding, K.; Shi, T.; Li, Q.; Wang, J. Improving land use/land cover classification by integrating pixel unmixing and decision tree methods. *Remote Sens.* **2017**, *9*, 16. [[CrossRef](#)]
25. Sun, S.; Liu, T.; Wang, Y.; Zhang, G.; Liu, K.; Wang, Y. High-rate underwater acoustic localization based on the decision tree. *IEEE Trans. Geosci. Remote Sens.* **2022**, *60*, 1–12. [[CrossRef](#)]
26. Virovlyanskii, A.L.; Zaslavskii, G.M. Ray and wave chaos in problems of sound propagation in the ocean. *Acoust. Phys.* **2007**, *53*, 282–297. [[CrossRef](#)]
27. Bertsimas, D.; Dunn, J. Optimal classification trees. *Mach. Learn.* **2017**, *106*, 1039–1082. [[CrossRef](#)]
28. Teixeira, A. Classification and regression tree. *Revue Des Maladies Respiratoires* **2004**, *21*, 1174–1176. [[CrossRef](#)] [[PubMed](#)]

Disclaimer/Publisher’s Note: The statements, opinions and data contained in all publications are solely those of the individual author(s) and contributor(s) and not of MDPI and/or the editor(s). MDPI and/or the editor(s) disclaim responsibility for any injury to people or property resulting from any ideas, methods, instructions or products referred to in the content.